Intelligent Adaptive Filtering Algorithm for Electromagnetic-Radiation Field Testing

Liu Sheng, Wang Bangmin, and Zhang Lanyong

***Abstract*—To reduce the effect of background noise on the electromagnetic-radiation field testing of large- and medium-sized equipment, this work combines the multiscale wavelet transform, particle swarm parameter optimization, and adaptive filtering algorithm improvement to obtain an intelligent adaptive filtering algorithm that can be applied to electromagnetic-radiation field tests. After these improvements, the new algorithm overcomes the problem of traditional algorithm in which the latter cannot ensure both convergence speed and steady-state error that satisfy the real-time requirements of field tests. The multiscale wavelet analysis segments and reconstructs the electromagnetic radiation and background noise of equipment within the frequency domain, and decomposes the broadband signal into a narrowband signal to overcome the difficulty in configuring broadband-signal filtering parameters. The particle swarm parameter optimization uses error $E[e^2(n)]$ as a fitness function to optimize the adaptive algorithm parameters, simplifying the operations performed by engineering personnel. The algorithm is simulated, and the actual engineering experimental data are verified in the Laboratory Virtual Instrument Engineering Workbench software platform, which prove that the proposed algorithm is more suitable to practical engineering application than the traditional adaptive filtering algorithm.**

***Index Terms*—Adaptive filtering, Laboratory Virtual Instrument Engineering Workbench (LabVIEW), noise elimination, particle swarm optimization (PSO), wavelet transform.**

I. Introduction

ELECTROMAGNETIC-RADIATION field test of large- and medium-sized electrical equipment is important to confirm the performance of its electromagnetic compatibility (EMC) during product development. The test site has a large effect on the test results, therefore, the EMC standard sets strict regulations about the test sites. The standardized test sites consist of an anechoic chamber (AC), open-area test site (OATS), and reverberation chamber (RC). For large- and medium-sized electrical equipment, a test in an AC cannot be always performed due to the equipment dimensions, operating requirements, and equipment installation. In addition, the construction expenses in AC become a significant limiting factor. Compared with AC, RC has a relatively low cost, is suitable for radiation immunity test, and is not appropriate for radiation emission test[1]. OATS is increasingly polluted by all types of ambient noise. Furthermore, OATS in remote areas are not beneficial for large- and medium-sized electrical equipment. Developing a method to perform electromagnetic-radiation field test of large- and medium-sized electrical equipment in the presence of ambient noise is therefore necessary.

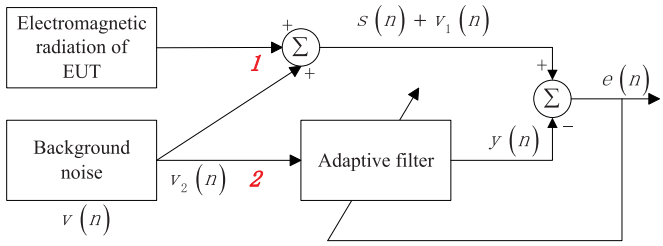

Fig. 1. Structure in filtering out the background noise of EUT.

The adaptive noise cancelation (ANC) technique in time-domain electromagnetic interference (TDEMI) measurement system is a good choice to suppress ambient noise, as presented in [2]. This system combines the ANC technique with the TDEMI measurement system. Thus, the measurement time spent in the presence of ambient noise between tests can be reduced by several orders of magnitude. The ANC technique can extract the radiated emission signal of the equipment from ambient noise without any prior knowledge about the noise signals, whose core element is an adaptive filter. Two antennas are used to simultaneously measure the signals. One antenna is used to receive the signal $s(n)$ of the equipment under test (EUT), and ambient noise signals $v_1(n)$ are located close to the EUT. The other antenna is used to capture only the ambient noise signals $v_2(n)$ and is installed far from the EUT. The second signal is filtered $y(n)$ and then subtracted from the first signal. The filter is adjusted to minimize the mean square of the difference $e(n)$ in the signals. The above principle of adaptive filtering is shown in Fig. 1.

Some research works have been done on the application of adaptive filtering algorithm in complex engineering environments. In [3], Osterwise *et al.* applied an adaptive noise cancellation technology to cancel the ambient electromagnetic

Manuscript received September 6, 2016; revised December 22, 2016; accepted January 13, 2017. Date of publication March 2, 2017; date of current version August 17, 2017. This work was supported in part by the National Natural Science Foundation of China subsidization under Project 51579047, in part by the National Key Technology Support Program under Grant 2013BAG25B01, in part by the Research Fund for the Doctoral Program of Higher Education under Grant 20132304120015, in part by the Doctoral Scientific Research Foundation of Heilongjiang under Grant LBH-Q14040, in part by the National Defense Fundamental Research Funds under Grant IEP14001, in part by the Open Project Program of the State Key Laboratory of Millimeter Waves under Grant K201707, and in part by the Fundamental Research Funds for the Central Universities under Grant HEUCF160414.

The authors are with the College of Automation, Harbin Engineering University, Harbin 150001, China (e-mail: liu.sch@163.com; 1442041178@qq.com; zlyalf@sina.com).

Color versions of one or more of the figures in this paper are available online at http://ieeexplore.ieee.org.

Digital Object Identifier 10.1109/TEMC.2017.2656896

interference (EMI) from near-field measurements of a clocked-logic electronic device taken in a noisy environment. This method used a block-processing adaptive filtering algorithm in the time domain. Frech and Russer[4] presented a real-time measurement system that performed ultrafast emission measurements in the range from 30 MHz to 1 GHz in the presence of ambient noise by combining the time-domain technology with the adaptive filter techniques. Xu *et al.* [5] briefly described the implementation process of the EMI measurements in the frequency domain using an adaptive filtering algorithm.

While applying ANC technique to large- and medium-sized electrical equipment encounters great difficulties in practical engineering as follows:

1) Poor ability to handle a relatively wide frequency band. Generally, the electromagnetic-radiation band of large- and medium-sized equipment is wide, the ambient noise is complex in the field test environment, and the noise spectrum is very wide. Although the adaptive filtering algorithm and its improved version can be solely used to obtain the optimal parameters of a single frequency simulation experiments, the known information about the equipment electromagnetic radiation in engineering applications shows that the interference signal has not only a single frequency but also a bandwidth. Therefore, satisfactory filtering effect cannot be achieved using only the unified optimal step.
2) It cannot ensure both convergence speed and steady-state error. In engineering practice, it cannot be applied to scenarios with high requirements in terms of real time and accuracy.
3) The parameter adjustment of the adaptive filtering algorithm requires professional knowledge, and it is difficult for nonprofessionals to perform.

In this paper, we proposed an intelligent adaptive algorithm used in electromagnetic radiated emission measurement of a large- and medium-size electrical equipment in the presence of ambient noise in the range of 9 KHz to 1 GHz. Based on ANC technology in TDEMI measurement system (described briefly in [6]), the intelligent adaptive algorithm combines modified least mean square (LMS) adaptive algorithm, wavelet transform together with particle swarm optimization (PSO). Our contribution can clearly been divided into four parts:

1) A novel structure of an adaptive filter is proposed. First, the signal received by the near-end antenna and that received by the far-end antenna are simultaneously split into adjacent frequency subband signals with different frequency widebands by wavelet transform, as described briefly in Section II. Second, the aforementioned subband signals in parallel are injected into each corresponding adaptive filter unit using four types of alternative modified adaptive algorithms whose parameters are optimized by the PSO algorithm. Finally, the output signal of each adaptive filter unit with the PSO algorithm is combined as the output of the entire intelligent adaptive filtering algorithm.
2) The proposed algorithm is applied to optimize the measurement of large- and medium-sized electrical equipment, which is seldom investigated as the target device because its test environment is more complex and the test bandwidth is wider. In particular, this algorithm can be used to reduce ambient noise below the 30 MHz frequency.
3) This work employs the PSO algorithm to obtain the parameters of the proposed algorithm.
4) To measure the radiated emission of large- and medium-sized equipment with wider bandwidth, we develop an EMI measurement system using the proposed intelligent adaptive algorithm, which is different from the other EMI measurement systems [7]–[9] presented in Section III.

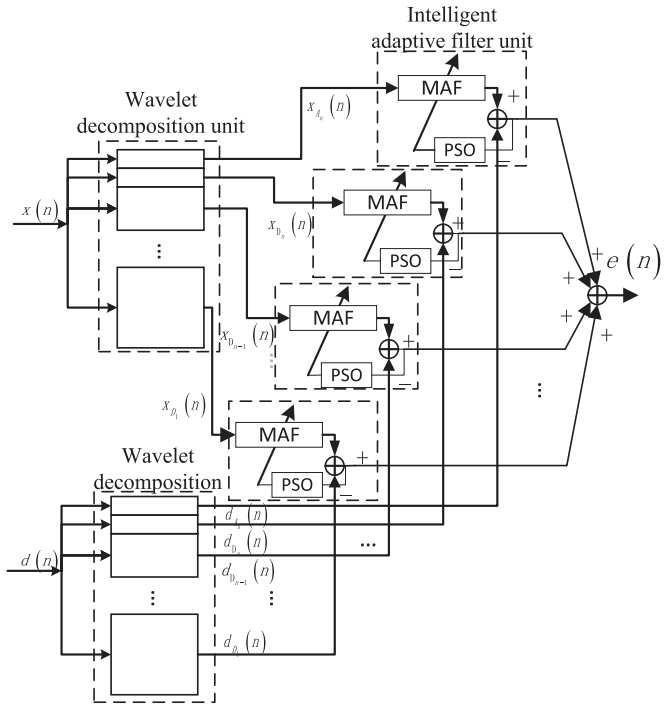

Fig. 2. Novel structure of the intelligent adaptive algorithm.

This paper is organized as follows: Section II introduces the proposed novel structure of the adaptive filter and briefly describes the components of this filter consisting of the wavelet decomposition and reconstruction method and the modified LMS adaptive algorithm. It also describes the PSO algorithm process to show the appropriate filtering parameters. Section III describes the exact setup of the experimental verification measurements and testing method. Section IV presents the comparison of the experimental results and analysis to verify the validity of the proposed algorithm. Conclusion is made in Section V.

II. Intelligent Adaptive Filtering Algorithm

The novel structure of the intelligent adaptive algorithm is shown in Fig. 2. Inspired by the adaptive filter based on wavelet transform [10]–[15] and practical application in the test, we combine the wavelet decomposition and reconstruction processes together with the adaptive filter using a novel structure to perform the test. First, both signals captured by two antennas are decomposed into a series of time-domain subband signals with

different bandwidths. Then, the modified LMS adaptive filter algorithm whose parameters are adjusted by the PSO algorithm is applied to these subband signals. Finally, the output of each filter unit is combined as the output of the entire structure. In Fig. 2, $x(n)$ and $d(n)$ denote the signals received by the far-end antenna and that received by the near-end antenna, respectively. MAF represents the modified adaptive filter algorithm, PSO represents the PSO algorithm. Symbols A and D represent the approximation and detailed information, respectively. The wavelet decomposition method will be briefly introduced.

Fig. 2 shows that the principal idea of the intelligent adaptive filtering algorithm is to implement a full-band filter by individually adapting each subband filter using the subband signals of input signals $x(n)$ and $d(n)$. The intelligent adaptive algorithm is similar to but is significantly different from the subband filter [15], [16], where the reference and the desired signals are first filtered by the filter banks and the outputs are then downsampled. At this time, both the signals are broken down into adjacent frequency subbands. Adaptive filtering algorithm is then applied to these signals. In our proposed intelligent adaptive algorithm, we first split the reference and the desired signals into adjacent frequency subbands using the filter banks. Second, each subband signal is subsampled. Third, each subband signal is upsampled and reconstructed using the synthesis filter bank. Next, the algorithm is applied to these signals. This procedure is shown in Fig. 2.

A. Modified Adaptive Filtering Algorithm

Although the LMS adaptive filtering algorithm is extensively applied in the ANC technique owing to its flexibility, extensibility, and simplicity in implementation, the various enhancements and variations discussed in this section are primarily a consequence of the contradiction between the convergence speed and steady-state error of the standard LMS adaptive filtering algorithm.

To overcome the contradiction, many modified algorithms have been investigated. In [17], Chen *et al.* established a nonlinear relationship between size step μ and error signal $e(n)$ based on the translation transformation of the sigmoid function. Roy and Shynk [18] added an incremental quantity to the weight-vector updating formula of the standard LMS algorithm. The modified algorithm is called the momentum LMS (MLMS) algorithm. Slock [19] presented the normalized LMS (NLMS) algorithm and compared the convergence behavior between the NLMS and LMS algorithms. Furthermore, the study on adaptive filter based on wavelet transform [10], [14], [20] and subband adaptive filtering [15], [21], [22] attracted our attention. On the basis of the modified LMS adaptive filtering and PSO algorithms, we propose the intelligent adaptive filtering algorithm by integrating the subband adaptive filtering into the wavelet transform.

In electromagnetic radiated emission test with high requirements in terms of real time and accuracy of large- and medium-sized equipment, the modified algorithm adopted by the intelligent adaptive filtering algorithm should have a quick convergence speed at the initial stage of the algorithm and a smaller steady-state error when the algorithm has converged.

In this section, we first briefly introduce some modified LMS algorithms. On one hand this process contributes to the implementation of the intelligent adaptive filtering algorithm in the EMI measurement. On the other hand, the parameter range of the modified algorithms is crucial to subsequent PSO (we shall separately provide the details in selecting the parameter application to the PSO algorithm later). Second, a series of simulations of the above-mentioned algorithms is performed to determine which algorithm will be selected in the filtering unit of the intelligent adaptive filtering algorithm. The modified LMS algorithms that involve the intelligent adaptive filtering algorithm consist of the sigmoid variable step-size (SVS) LMS, MLMS, and extended (ELMS) algorithms. For completeness of this paper, we summarize the MLMS, SVSLMS, and ELMS algorithms.

The MLMS algorithm corresponds to a second-order adaptive algorithm in that two previous weight vectors are combined in each iteration to obtain the updated weight vector as follows:

$$W(n+1) = W(n) + 2\mu e(n)X(n) + \alpha[W(n) - W(n-1)] \tag{1}$$

where $W(n) = [w_0(n), \ldots, w_{N-1}(n)]^T$ denotes the weight vector and the output error is given by $e(n) = d(n) - W^T(n)X(n)$. $X(n) = [x_0(n), \ldots, x_{N-1}(n)]^T$ is the input vector, $d(n)$ is the (scalar) desired response, and $y(n) = W^T(n)X(n)$ is the corresponding estimate of $d(n)$. Step size μ controls the convergence rate, and new parameter α scales the momentum term added to the gradient descent, where $|\alpha| < 1$. The behavior of the MLMS algorithm was analyzed in detail in [18].

The SVSLMS adaptive algorithm is derived from the standard LMS adaptive algorithm by building a nonlinear relationship between step size $\mu(n)$ and error signal $e(n)$ as follows:

$$\mu(n) = \beta\left(\frac{1}{1+\exp(-\alpha|e(n)|)} - 0.5\right) \tag{2}$$

where α is bounded as $\alpha > 0$ and β is bounded as $0 < \beta < \frac{1}{1+\lambda_{\max}}$ in which $\lambda_{\max}$ is the maximum eigenvalue of the input signal autocorrelation matrix, which is constant and controls the shape and range of the values of this function.

The ELMS adaptive algorithm is a modified SVSLMS algorithm based on a sliding window. Variable-step size $\mu(n)$ and updated weight vector $W(n)$ are, respectively, given by the following equations at each iteration as follows:

$$\mu(n) = a\left(1 - \frac{1}{b|e(n)e(n-1)|^r}\right) \tag{3}$$

$$W(n+1) = W(n) + 2\mu(n)[e(n) - \alpha_1 e(n-1) - \alpha_2 e(n-2)]X(n) \tag{4}$$

where $0 < a < \frac{1}{\lambda_{\max}}$, $b > 0$, and $r > 0$ are constants used to control the shape and the range of values of the step-size curve and both α_1 and α_2 under constraint $\alpha_1 + \alpha_2 = 1$ are the factors of the sliding window error estimation.

Although the analysis of the aforementioned adaptive filtering algorithms has been proposed in some references, it is also

TABLE I
PERFORMANCE COMPARISON BETWEEN STANDARD AND IMPROVED ALGORITHMS

Algorithm \ Index	Parameter Configuration	Convergence Speed /Iteration Times	Steady-State Error (dB)	Stability
Standard LMS algorithm	$N = 2$ $\mu = 0.7$	900	-42.5	Stable
SVSLMS algorithm	$a = 2000$ $b = 0.4$	200	-41.3	Stable
Order-changing LMS algorithm	$N = 150$ $\mu = 0.007$	1300	-38	Stable
MLMS with momentum term	$\mu = 0.01$ $\alpha = 0.34$	500	-44.0	Stable
ELMS	$\alpha_1 = 0.9$ $\alpha_2 = 0.1$ $a = 0.1$ $b = 210$ $r = 1$	1900	-43.5	Stable

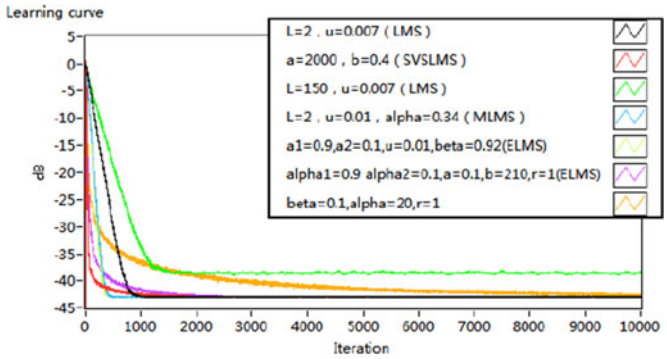

Fig. 3. Simulation learning curve.

essential to compare the convergence rate and steady-state error by simulations to select the proper adaptive filter algorithm in the proposed method. In this section, we will concentrate on the two characteristics of an adaptive filter, namely its convergence behavior and steady-state error, which remain after the algorithm has converged.

The simulation conditions are set as follows:

1) Desired signal $s(n) = 0.01 \times \sin(\pi n/1000); n = 0 : 10000$ is a sine-wave sequence using 10 000 samples.
2) Reference input signal $v_2(n)$ is a Gaussian noise with zero mean and a variance of $\sigma^2 = 1$.
3) $v_1(n)$ is a Gaussian noise with a zero mean and a variance of 0.1.

In terms of simulations, there is no a certain criterion to determine the optimal parameters, so the parameter selection of the aforementioned algorithms become extraordinary hard. We determine the parameters of each algorithm by practical experience. The solution to this problem is presented in Section II-C.

The above signals are processed by the LMS, SVSLMS, MLMS, and ELMS algorithms, respectively. The parameters of the LMS algorithm consist of the order of filter $N = 2$, and step size $\mu = 0.007$. A small step size can decrease the steady-state error, but makes the convergence rate slow. What's more, we maintain step size and set $N = 150$ to examine the effect of the order of adaptive filter on the performance of LMS algorithm. This conclusion can be proved in the simulation. The parameters of SVSLMS algorithm are set to $N = 2, \alpha = 2000, \beta = 0.4$. The MLMS algorithm with $N = 2, \alpha = 0.34, \mu = 0.01$ and the ELMS algorithm with $\alpha_1 = 0.9, \alpha_2 = 0.1, a = 0.1, b = 210, r = 1$, and $N = 2$ are used. The aforementioned algorithms, their parameters, and performance are induced in Table I. Note that parameters for the above algorithms are selected based on a large number of simulations. Compared with other parameters of individual algorithms, the selected parameters is relatively optimal.

By conducting 1000 times of independent simulations using 10 000 samples each time, we obtained the statistical average and learning curve, as shown Fig. 3.

In Fig. 3, as compared to LMS ($N = 2, \mu = 0.007$), which is taken as the standard reference, we can observe that LMS ($N = 150, \mu = 0.007$) has slow convergence rate and large steady-state error with the order increase, SVSLMS ($N = 2, \alpha = 2000, \beta = 0.4$) can obtain smaller convergence rate and slightly reduce the steady-state error, MLMS ($N = 2, \alpha = 0.34, \mu = 0.01$) keep a good balance between the convergence rate and the error. What's more, though decreases the error, ELMS ($\alpha_1 = 0.9, \alpha_2 = 0.1, a = 0.1, b = 210, r = 1$, and $N = 2$) is time consuming. Qualitative analysis is presented briefly in Table I.

According to the above analysis of the algorithm, the MLMS, SVSLMS, and ELMS algorithms based on different modified methods in the context of the standard LMS algorithm can overcome the contradictory between the convergence rate and the steady-state error.

A qualitative analysis of Fig. 3 shows that the improved algorithms improve the convergence speed and steady-state error to varying degrees. Furthermore, the quantitative analysis results listed in Table I shows that the MLMS algorithm with a momentum term has a better effect in balancing the convergence speed and steady-state error than the other algorithms. Under the same simulation conditions, the MLMS algorithm can converge in approximately 500 steps and has a minimum steady-state error. Therefore, this study uses the MLMS algorithm with a momentum term as the core adaptive filtering algorithm to overcome the contradiction between the convergence speed and steady-state error in practical applications.

Although the results of the simulations show that the MLMS algorithm has the best performance in terms of the convergence rate and mean square error (MSE), other algorithms such as the SVSLMS and ELMS algorithms can possibly adjust their parameters so that their learning curve shows similar performance to the MLMS algorithm. We still consider both algorithms as alternative algorithms. In summary, because of the complexity of the actual signals, the results of the simulation are not very much consistent with those of the practical experiment. Hence, applying which algorithm to use in the proposed structure of the adaptive filter depends on the comprehensive analysis of the results of the simulations and the practical experimental verification. The purpose of the simulation is to demonstrate that the modified algorithm can overcome the contradiction between the convergence rate and steady-state error; thus, we applied scenarios with higher requirements in terms of real time and accuracy. In addition, we can see that no proper method is available to select the parameters for the modified LMS algorithm in

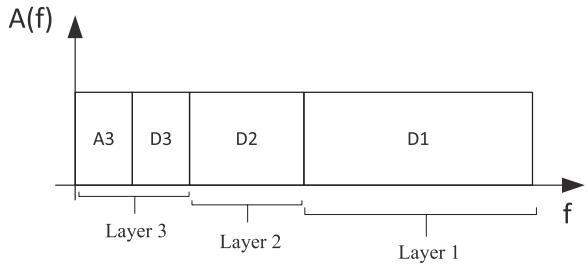

Fig. 4. Example of wavelet decomposition.

the simulation process. We can only rely on the empirical and large number of simulations. In view of this situation, we plan to apply the PSO algorithm to the intelligent adaptive filtering algorithm to overcome the drawback.

B. Wavelet Decomposition

In this section, we show how to apply the wavelet transform to perform signal $X(n)$ and $d(n)$ decomposition and reconstruction.

Wavelet transform integrated with adaptive filtering algorithm has been investigated in some references. In [13], orthogonal wavelet transform whitens the input signal of the LMS algorithm to improve the performance of the algorithm. What makes the proposed algorithm different from the existing adaptive algorithm in the wavelet domain [10] is that signals $X(n)$ and $d(n)$ are simultaneously decomposed through the wavelet transform, rather than simply decomposing signal $X(n)$. The advantage is that we can employ the appropriate modified LMS algorithm for each intelligent adaptive filter unit according to the spectrum characteristic of the subband signals.

Because the conventional LMS adaptive filtering algorithm processes the received data using a step size for the entire frequency band, it can unlikely achieve better filtering performance than applying the adaptive algorithm to each subband because in each sub band, the adaptation step size can be matched to the energy of the input signal in that band.

The goal of the proposed wavelet decomposition is to split the wideband signals into sub bands, filter the subband signals using the modified LMS algorithm whose parameters can be adjusted by the PSO algorithm, and finally output the filtered signal. At this moment, the output signal is regarded as the exact radiated emission of the device under test (DUT). We can note that the wavelet decomposition unit of the intelligent adaptive filtering algorithm can decompose a signal according to the level that we specify and reconstruct the signal from the frequency bands that we desire. For instance, a signal is split into three levels by wavelet transform, as shown in Fig. 4, where symbols A and D represent the approximation and detailed information, respectively. The subscript of the symbol represents which level it belongs to. We can see that the frequency bands decomposed by the wavelet transform are not uniform. The lower the frequency is, the narrower is the frequency band. The characteristic of the wavelet transform matches in a small step with the narrow frequency band, which improves the convergence performance of the adaptive filtering algorithm.

To improve the poor ability of the traditional LMS adaptive filtering algorithm in processing a wideband signal and noise, we divide the wideband into smaller bands before adaptive filtering. Wavelet transform can provide multiresolution analysis and time–frequency localization, which can decompose the wideband signal into narrow bandwidths. Considering the practical application of the wavelet transform in the intelligent adaptive algorithm, a study on the wavelet transform and its implementation is greatly necessary. In the following discussions, we provide a brief introduction on the wavelet transform.

The wavelet transform uses a signal and a set of wavelet basis as inner products, and the common tools include continuous and discrete wavelets. The continuous wavelet is mainly used for signal analysis, and the discrete wavelet is mainly used for signal analysis and processing such as noise filtering, data compression, peak detection, and signal analysis in different scales

$$WT_{u,a} = \int_{-\infty}^{+\infty} s(t)\Psi_{u,a}^{*}(t)dt \tag{5}$$

where

$$\Psi_{u,a} = \frac{1}{\sqrt{a}}\Psi\left(\frac{t-u}{a}\right). \tag{6}$$

$WT_{u,a}$ indicates the wavelet coefficient, $\Psi_{u,a}$ includes the wavelet basis, u indicates the displacement factor, and a indicates the scale factor of the wavelet basis.

The wavelet transform possesses the following characteristics: the small scale has a small time range, wide frequency band, and higher central frequency; and the contrast scale has a long time range, narrow frequency band, and lower central frequency. The time range and frequency band determine the time–frequency resolution of the wavelet function. A long time range indicates a rough time resolution, and a wideband indicates a rough frequency resolution.

The three main reasons why wavelet transform is rarely used in practice are as follows:

1) Usually, the real signal that we encounter can be used only after discrete-time sampling, and the analog signal input form of $s(t)$ cannot be obtained at all.
2) Except in very rare cases, the integral of the integrand does not exist.
3) Although the numerical algorithm can be used to calculate the coefficient of continuous wavelet, the biggest problem of the continuous wavelet is that the signal cannot be restored by reconstruction, which is inconsistent with the objective of processing the signal to finally obtain a time-domain signal in practical applications.

The wavelet decomposition unit, which is based on the Mallat algorithm [11], [23] and is applied in the intelligent adaptive filtering algorithm, consists of the decomposition and reconstruction stages. It is briefly introduced as follows.

In the decomposition stage, a series of coefficient sets is produced, and each of them denotes the information of the signal in different scales. As shown in Fig. 5, considering three levels as an example, original signal s produces two sets of coefficients, namely detail coefficient vector D_1 and approximation

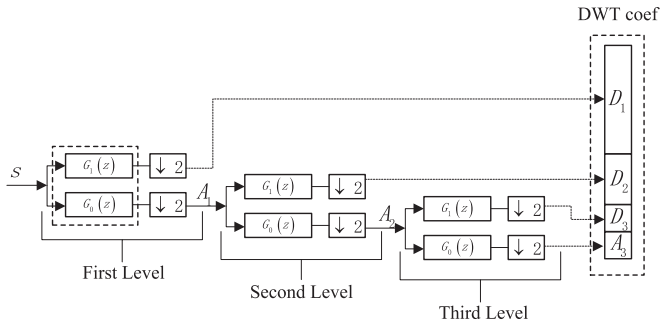

Fig. 5. Principle of the discrete wavelet decomposition.

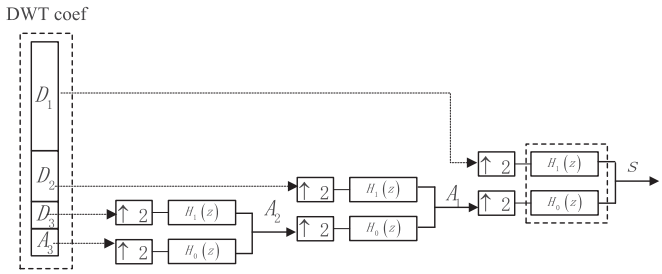

Fig. 6. Principle of the discrete wavelet reconstruction.

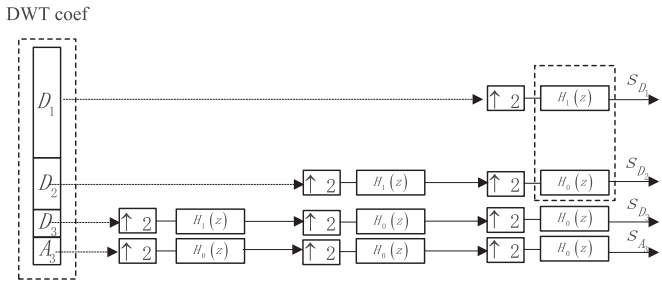

Fig. 7. Structure of the intelligent algorithm reconstruction.

coefficient vector A_1. These vectors are obtained by convolving with high-pass filter $G_1(z)$ for details and with low-pass filter $G_0(z)$ for approximation, followed by dyadic downsampling. $G_1(z)$ and $G_0(z)$ form the decomposition filter bank. D_2, D_3, A_3 and are obtained in the same manner. The reconstruction stage performs the reverse operation to that in the decomposition stage, as shown in Fig. 6.

To obtain the reconstructed signal corresponding to A_3, first, we reserve the approximation coefficient vector A_3, and the remaining coefficient vectors are set to zero. Second, the aforementioned coefficient vectors are reconstructed during the reconstruction stage of the Mallat algorithm. We can obtain the reconstructed signals of D_1, D_2, and D_3 in the same manner. The reconstruction process thereby reverts to the structure, as shown in Fig. 7. In the above scheme, we can extend the three levels of processes to an arbitrary number.

So far, we have implemented the goal of splitting the wideband signals to a series of subband signals whose frequency band is not uniform. The two crucial factors of the wavelet decomposition unit, namely the level and wavelet functions, determine the number and characteristic of the subband signals, respectively. Because the radiated emission signal of the large- and medium-sized equipment have a wider frequency band, the results of the repeated simulation show that the proper number of levels is 11, and the proper wavelet basis is Daubechies 2 for spectrum slicing of the signals with background and reference channel noises. The application of the two parameters for intelligent adaptive filtering algorithm is presented in Section II-C.

C. Parameter Selection Based on the PSO Algorithm

In this section, we consider that the PSO algorithm is applied to the parameter selection problem. The adaptive filter based on the PSO algorithm has been widely used in practical engineering to overcome the difficulty in the adaptive filter parameter adjustment. In [24] and [25], the PSO algorithm was successfully individually applied to the adaptive filtering and adaptive infinite impulse response structure. In addition, the PSO algorithm in electromagnetics is presented in [26]. The motivation for the investigation of the PSO algorithm as applied to parameter selection in the adaptive filtering algorithm is that the process relies on experience without a reliable theoretical basis on one hand. On the other hand, nonprofessionals have difficulty performing this process on practical electromagnetic radiated emissions of the large- and medium-sized electrical equipment. Unlike the aforementioned references on the application of the PSO algorithm in adaptive filtering algorithm, the proposed intelligent adaptive filtering algorithm concentrates on the parameter selection based on the modified LMS algorithm, and these selected parameters are derived from the gradient descent algorithm. In contrast, the approach used in [25] did not calculate the gradient but directly searched the optimal weight vector according to the fitness function.

To better introduce the basic idea of the intelligent adaptive filtering algorithm in the parameter selection, we need to outline the PSO algorithm.

The PSO algorithm is an evolutionary algorithm, which starts with the initialization of a swarm of M particles with random velocity and position vector. Dimension R of the velocity and position vector represents the number of unknown parameters to be optimized. At each iteration, the fitness of each particle is first calculated according to the cost function (i.e., MSE), restored, and progressively replaced by the most fitting parameters of each particle (called $p\text{best}_i, i = 1, 2, \ldots, M$) as well as a single most fitting particle ($g$best) as better fitting parameters are encountered. Each particle (p_i) updates its velocity and position as follows:

$$\begin{aligned}\text{vel}_i(n) = {} & w * \text{vel}_i(n-1) \\ & + \text{acc}_1 * \text{diag}[e_1, e_2, \ldots, e_R]_{i1} * (g\text{best} - p_i(n-1)) \\ & + \text{acc}_2 * \text{diag}[e_1, e_2, \ldots, e_R]_{i2} * (p\text{best}_i - p_i(n-1))\end{aligned} \tag{7}$$

$$p_i(n) = p_i(n-1) + vel_i(n) \tag{8}$$

where $\text{vel}_i(n)$ denotes the velocity of the ith particle, e_r represents random values in the range from zero to one, acc_1 and

acc_2 are the acceleration coefficients toward $g\text{best}$ and $p\text{best}_i$ respectively, and w is the inertia weight, which controls the influence of the previous velocity on the current velocity. For more details, please refer to [24].

On this basis, our goal is how to apply the PSO algorithm to the parameter selection. Two critical factors are present, namely the solution space and the fitness function, which show the relationship between the PSO algorithm and the practical parameter selection problem. Thus, these must be specified in each optimization. The rest of the implementation is independent of the practical problem [26]. For this reason, the subject of this section is the discussion on how to connect the PSO algorithm with the parameter selection of the modified LMS algorithm, instead of the remaining implementation, independent of the practical problem. The modification of the PSO algorithm itself has been investigated in [27] and [28].

The modified LMS adaptive algorithms are similar in nature in terms of the parameter selection. We therefore consider the MLMS algorithm as an example to describe the two aforementioned critical factors. The parameters of the MLMS algorithm that include step size μ, momentum factor α, and filter order N must be adjusted. The filter is essentially designed to optimize the multiple parameters. The PSO algorithm is used to efficiently and concurrently search the entire parameter space to obtain the best parameter values, where α is the momentum factor with a range of $|\alpha| < 1$, μ is a step size with a range of $0 < \mu < \frac{\alpha}{1+\lambda_{\max}}$, $\lambda_{\max}$ is the maximum eigenvalue of the input signal autocorrelation matrix, and N is a positive integer not less than two. Obviously, this is an issue in PSO for mixed integer programming. Two key points are considered in the algorithm design as follows:

1) Selecting the adaptive function (currently, the commonly used adaptive function is the mean square deviation of the adaptive filter).
2) Rounding up/down filter order *N* to obtain an integer.

Currently, the commonly used methods include direct, random, and eventual rounding. The design in this work uses the direct-rounding method, i.e., it uses the particle swarm algorithm to calculate the position of each particle. When the particles arrive at a position, we immediately round up/down the location parameter values of each particle, calculate their fitness values, extract the optimal positions of the particle and the global particles, and start the next rounding cycle until the calculation results satisfy the requirements.

After introducing the two critical factors, which are encountered PSO issues in mixed integer programming and its solutions, we summarize the application of the PSO algorithm to the parameter selection of the modified LMS algorithm as follows:

Step 1: The parameters of the modified LMS algorithm are selected and provided with a range of values, as briefly introduced in Section II-A.

Step 2: We initialize the swarm; then, the number of particle swarm M, acceleration coefficients acc_1 and acc_2, and inertia weight w are determined.

Step 3: We evaluate the fitness of each particle. We choose the MSE as the fitness function.

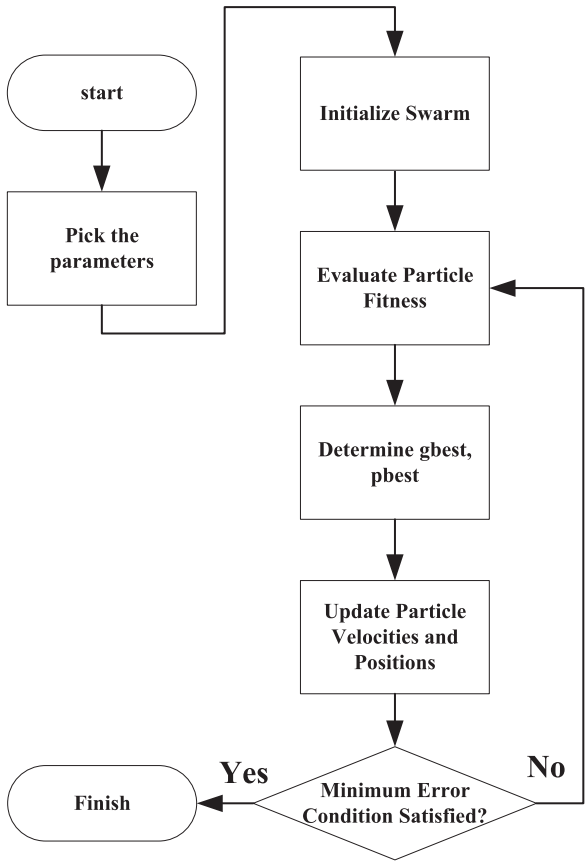

Fig. 8. Flowchart of the PSO algorithm.

Step 4: We restore and progressively replace the most fitting parameters of each particle as well as the single most fitting particle when better fitting parameters are encountered.

Step 5: We update the velocity and position of each particle according to (7) and (8).

Step 6: If a stop criterion is satisfied (MSE is sufficiently small) or a predefined number of iterations are arrived, the iteration process ends. Otherwise, the system returns to Step 3.

The flowchart is shown in Fig. 8.

In summary, the proposed intelligent adaptive filtering algorithm uses the discrete wavelet transform to simultaneously decompose the signals that contain ambient noise and the radiated emissions of the equipment with ambient noises to multilayer wavelets. It then decomposes the signals into different frequency bands and reconstructs each band. Consequently, it uses the modified LMS algorithm to process the data in each layer for adaptive filtering, employs the PSO algorithm to optimize the parameters of the modified LMS algorithm, and eventually synthesizes the data in each layer after filtering to obtain the electromagnetic-radiation signal without ambient noise. The specific algorithm flowchart during the intelligent adaptive filtering stage is shown in Fig. 9.

III. Experimental Verification

To verify the performance of the proposed intelligent adaptive filtering algorithm, the practical data from the electromagnetic radiated emissions of the large- and medium-sized electrical

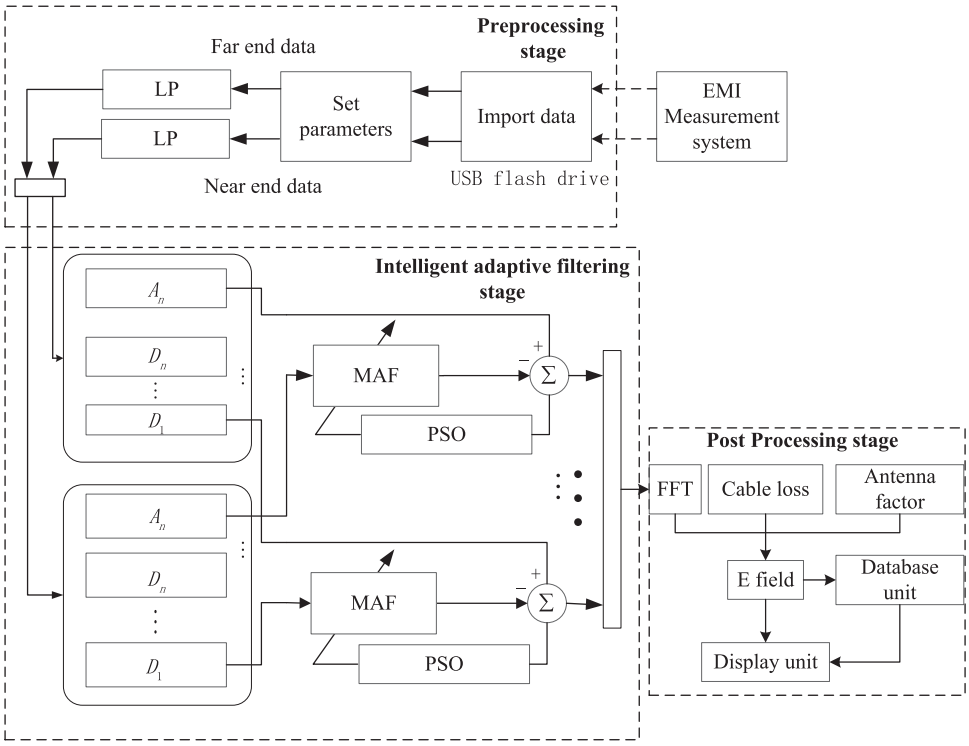

Fig. 9. Filtering flowchart of the algorithm.

equipment with ambient noise are used. For comparison, we also obtain the data from the equipment in AC. We select large- and medium-sized electrical equipment as the target DUT because it has complex radiated emissions with a wide frequency band, which can help in testing the quality of the algorithm under severe environment. Note that once the large- and medium-sized electrical equipment is installed in AC, we can no longer move the equipment to prevent the test results from being influenced by irrelevant factors to a large extent during the entire experimental process.

In the next section, an EMI measurement system that uses the proposed intelligent adaptive filtering algorithm is constructed, which consists of three sets of antennas (two telescopic, two biconical, and two log-periodic antennas), two identical cables with 1-dB cable loss, and a Rohde & Schwarz RTO1044 oscilloscope with four channels. This system uses three sets of ultrabroadband antennas because the radiated emission signal of the large- and medium-sized equipment has a wide frequency band that ranges from 9 kHz to 1 GHz. Currently, an antenna with a frequency-band range from 9 kHz to 1 GHz has not yet been developed. Thus, the three types of antennas whose entire frequency bands cover the test frequency are combined to perform the test. We note that the frequency range from 9 kHz to 1 GHz has not been addressed by other EMI measurement systems (in [2] and [3], the frequency ranges of the addressed signals are from 30 MHz to 1 GHz and from 10 to 700 MHz, respectively), which is a significant feature of the EMI measurement system addressed in our current study. To reduce the effect of the confounding variables on the antenna performance to a large extent, two antennas with identical antenna factor for the telescopic, biconical, and log-periodic antennas are employed in the EMI measurement system, whereas both of them were calibrated before being used to simultaneously measure the signals. The three types of antennas and their test information are listed in Table II.

In addition, the intelligent adaptive filtering algorithm is implemented in the Laboratory Virtual Instrument Engineering Workbench (LabVIEW), where we design the software that consists of three stages: preprocessing, intelligent adaptive filtering algorithm, and postprocessing stages. In the preprocessing stage, the far- and near-end data and the data from the EMI measurement system are first imported into LabVIEW via a USB Flash drive, where the data are saved as .csv files. Second, the sampling frequency and storage depth are set according to Table II, and the two parameters significantly affect the performance of the fast Fourier transform (FFT). Third, the near- and far-end data are set to this frequency range corresponding to the test band of the selected antenna. In the intelligent adaptive filtering stage, the proposed intelligent adaptive filtering algorithm is implemented to cancel the ambient noise. In the postprocessing stage, the *E*-field strength of the equipment is given by the following equation:

$$E_f = V_f + \mathrm{AF}_{FS(f)} + C_{Rd} \tag{9}$$

where f is the frequency (MHz), E_f denotes the *E*-field at distance d from the source, expressed in dB (μV/m), $\mathrm{AF}_{FS(f)}$ is the antenna factor (dB(m^{-1})) obtained by the curve fitting in LabVIEW, and C_{Rd} is the cable loss. Then, the *E*-field strength of the radiated emissions of the equipment is displayed in the display unit, whereas the data are also saved in the database unit

TABLE II
TEST PARAMETER CONFIGURATION

Antenna type	Frequency range	Sampling frequency (Gsa/s)	Sampling time	Storage depth	Processing data
Telescopic antenna	9 kHz–60 MHz	1	1 ms	1 Mb	1 Mb
Biconical antenna	20–330 MHz	10	500 μs	5 Mb	1 Mb
Log-periodic antenna	200 MHz–1 GHz	10	500 μs	5 Mb	1 Mb

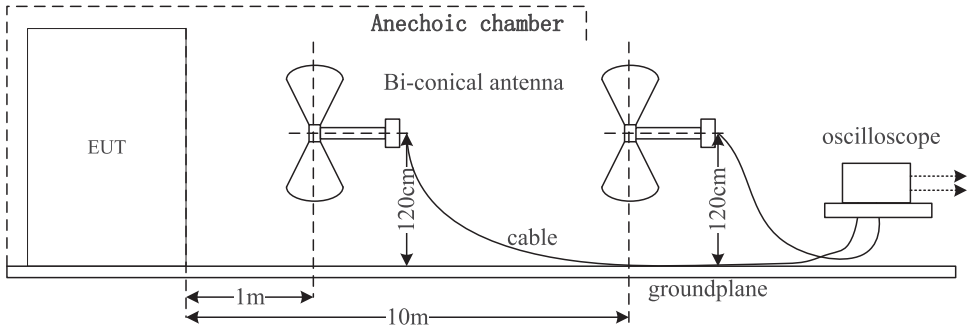

Fig. 10. Test in non-AC.

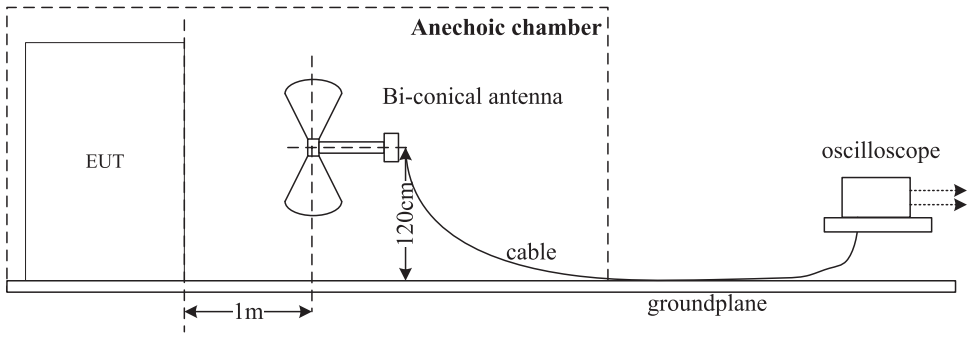

Fig. 11. Test in AC.

for data management and redisplay. The procedure is shown in Fig. 9.

A. Testing Environment and Testing Method

In this section, we use two antennas to perform the radiated emission test of a medium-voltage transformer as the target equipment in the presence of ambient noise, as shown in Fig. 10. Subsequently, this equipment is measured in a relatively noise-free environment in an AC using one antenna and a setup similar to that shown in Fig. 11, as shown in Fig. 10. Meanwhile, many types of electrical equipment are present outside the AC. Therefore, we can obtain or eliminate various types of external noise by turning ON or OFFthese electrical devices when we apply the adaptive filtering algorithm for ambient noise cancelation. This process enables the creation of various types of controlled background noise signatures to verify the effectiveness of the proposed algorithm.

We locate the medium-voltage transformer in the AC, turn it ON, wait until it enters the normal working state, and install a near-end antenna with $d = 1$ m (this equation denotes that the distance between the near-end antenna and the equipment is 1 m) in front of the equipment to capture the radiation signal. During the test, we close the door of the AC, connect the cable that leads from the AC to the Rohde & Schwartz oscilloscope beside the AC, set the test parameters according to Table II, save the data in the Rohde & Swartz oscilloscope as .csv files, and copy them to a USB Flash drive for subsequent data processing.

After the above-mentioned test, we turn the equipment OFFand keep the other settings unchanged, save the data in the Rohde & Swartz oscilloscope as .csv files, and copy them to a USB Flash drive for subsequent data processing. At this time, we perform the ambient measurement.

In the non-AC test, we keep the near-end antenna in the same position and place another antenna of the same type in a position nine times farther than the near-end antenna distance outside the AC to reduce its received electromagnetic-radiation signal. We ensure that the equipment, near-end antenna, and far-end antenna are in the same line. We open the door of the AC, introduce background interference, and keep the other

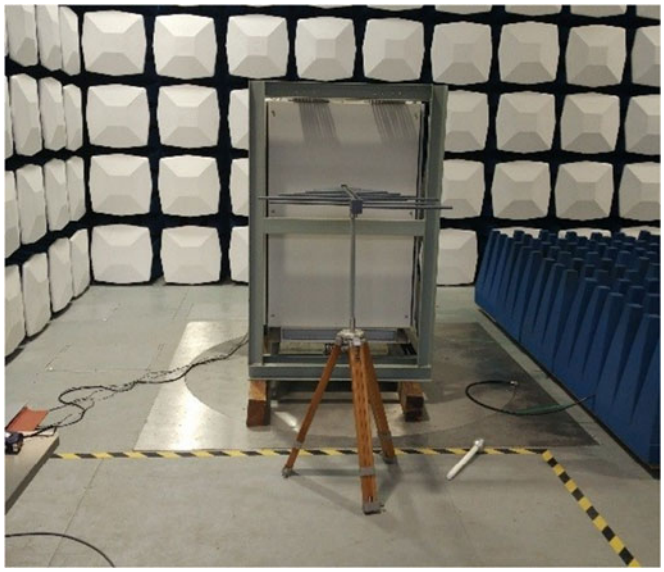

Fig. 12. Field test setup.

electrical equipment outside the AC in working state to increase the complexity of the test environment. Meanwhile, we can obtain or eliminate various types of external noise by turning ON orOFFthese electrical devices to control the ambient noise signatures. We place the Rhode & Schwartz oscilloscope between the two antennas, as shown in Fig. 12, and use cables to connect it to the antennas. We save the electromagnetic-radiation data in a.csv format and store them in a USB Flash drive for subsequent data processing. The structure diagram of the electromagnetic-radiation test for the medium-voltage transformer is shown in Fig. 10. Three types of antennas are used to successively perform the aforementioned tests. The difference is that different types of antennas correspond to different sampling frequency F_s and storage depth N, both of which determine frequency resolution $\triangle f$ according to the following equation:

$$\triangle f = \frac{F_s}{N} \tag{10}$$

where $\triangle f$ has a large effect on the performance of the FFT, sampling frequency F_s, and storage depth N, as listed in the Table II.

In summary, three tests are performed by developing an EMI measurement system. The ambient measurement is performed using a medium-voltage transformer with no power. The test of the energized medium-voltage transformer in the presence of ambient noise is also performed. Finally, the test with all equipment in the AC being energized is performed. In the following section, we will present the process that obtains the data using the proposed intelligent adaptive filtering algorithm to verify the algorithm performance.

IV. Measurement Results and Analysis

In this section, we present the validation of the effectiveness of the proposed intelligent adaptive filtering algorithm using the experimental results. We should note that the effectiveness of the proposed algorithm depends on whether the output results of the algorithm are consistent with the results in the AC. In addition, the conventional LMS algorithm is applied to verify the effectiveness of the proposed algorithm for comparison. To verify the effectiveness of the proposed algorithm for the electromagnetic radiated emissions in the presence of ambient noise *in situ*, quantifiable measurement is needed. The results obtained by the proposed algorithm are consistent with those of the measurement in the AC within a permissible error. When the maximum measurement error between the output spectrum results of the proposed algorithm and the AC is less than 2 dB in the frequency range from 9 kHz to 30 MHz and 6 dB in the frequency range from 30 MHz to 1 GHz, we consider that the proposed algorithm can be applied to measure the radiated emissions of the equipment in the presence of ambient noise instead of inside the AC.

First, the results of the proposed algorithm are compared with those of the conventional LMS algorithm to prove that the proposed algorithm shows a significant improvement. The results of the proposed algorithm are consistent with those of the AC test with permissible error. Thus, the proposed algorithm can be applied to measure the radiated emissions of the large- and medium-sized equipment *in situ* in the presence of ambient noise instead of in the AC in practical engineering.

A. Ambient Measurement With Unenergized DUT

When the equipment is turned OFF, the two telescopic antennas only received ambient noise. We can see that the spectrum of the ambient noise consists of a series of spikes in the range from 9 kHz to 3 MHz (the reason for the displayed frequency-band range from 9 kHz to 3 MHz instead of the measurement frequency-band range from 9 kHz to 30 MHz is that the spectrum above 3 MHz is relatively flat and low), which illustrates that the EMI caused by the equipment outside the AC is adequately complex and helps verify the effectiveness of the proposed algorithm under complicated environment. The proposed and the conventional LMS algorithms are used to process the received data. Theoretically, the ambient noise should have been perfectly cancelled. The results of the proposed algorithm shown in Fig. 13 are consistent with the theoretical results with a permissible error. Compared with the spectrum of the ambient noise, the conventional LMS algorithm that uses the parameters of step size $\mu = 7$ and order $N = 2$ can suppress the noise to some extent, but the results are unsatisfactory. We have proven that the proposed algorithm is more efficient than the conventional LMS algorithm; however, this is not sufficient. In the following, we will further investigate the effectiveness of the proposed algorithm.

As an example of the corresponding subband at level D_8, Fig. 13(c) shows the scheme of the proposed algorithm, i.e., the proposed algorithm achieves better performance by applying the modified LMS algorithm with the PSO algorithm to the received data in each sub band.

B. Test Results of Telescopic Antenna

When the equipment is turned ON, the two telescopic antennas are installed as shown in Fig. 10. We replace the two biconi-

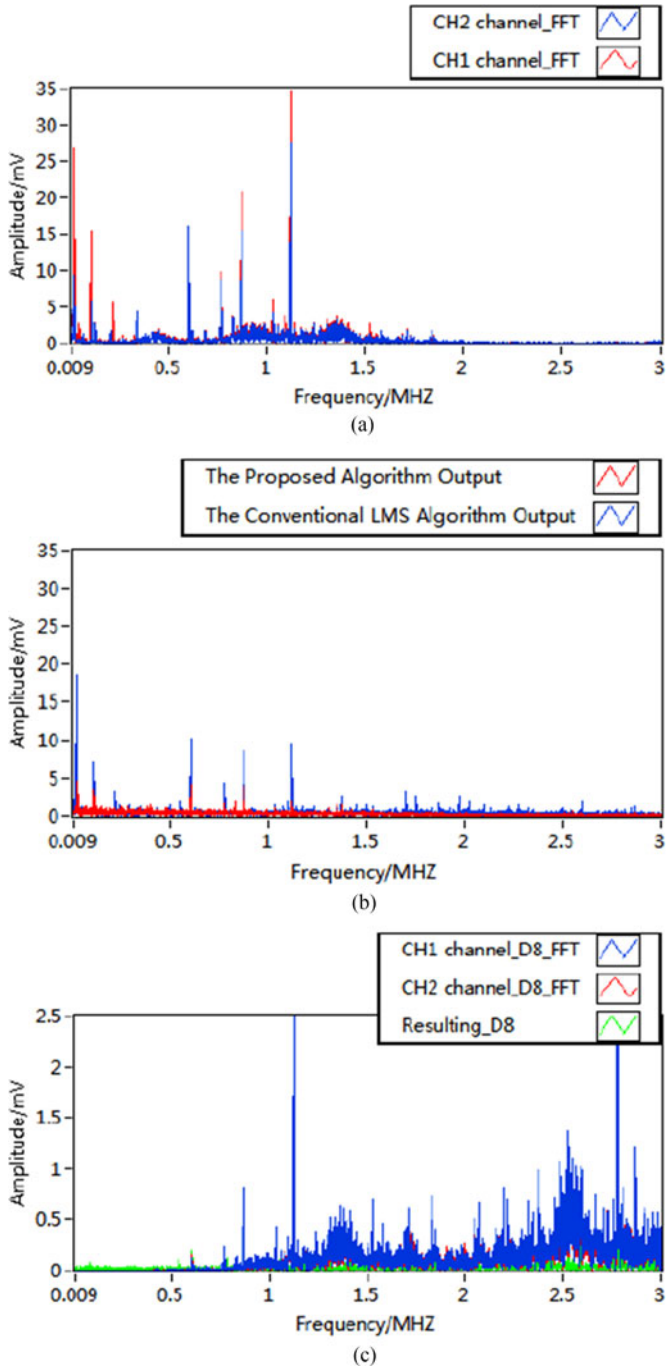

Fig. 13. Spectrum of the signal measured by a telescopic antenna. (a) Spectrum of the signal (containing background noise). (b) Spectrum of the signal after filtering. (c) Spectrum of the signal after filtering at level 8.

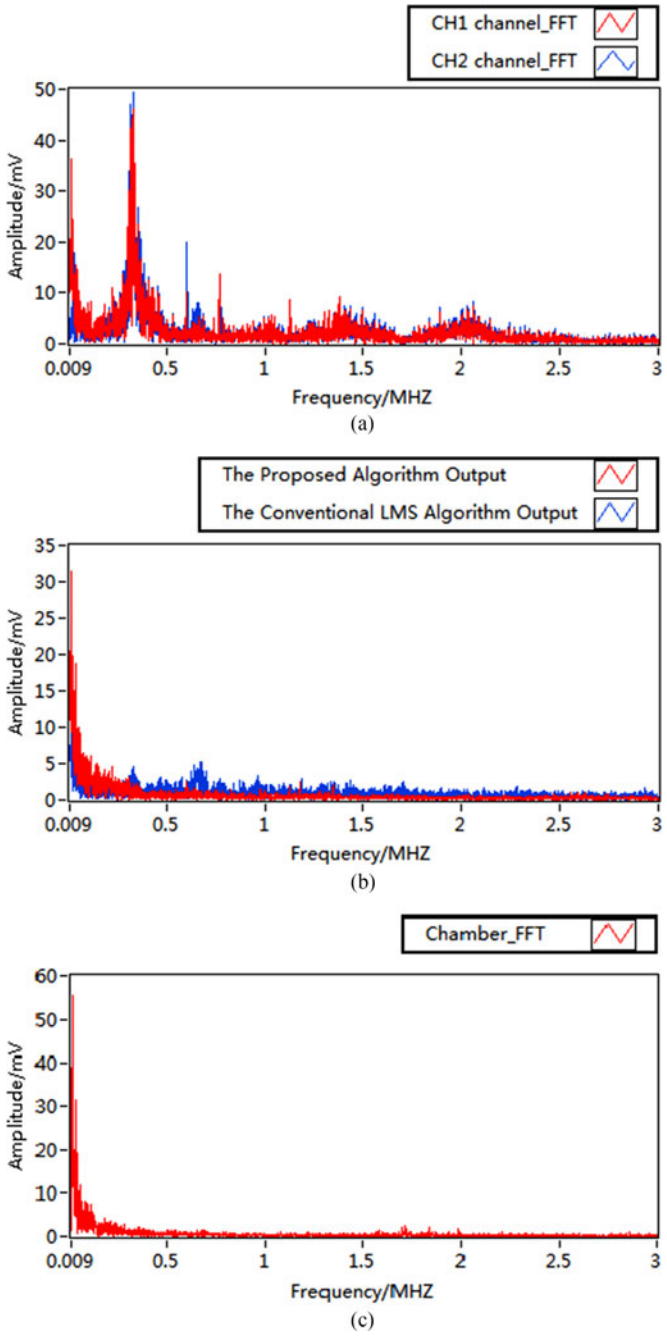

Fig. 14. Spectrum of the signal measured by a telescopic antenna. (a) Spectrum of the signal (containing background noise). (b) Spectrum of the signal after filtering. (c) Spectrum of the signal in the AC.

cal antennas with the two telescopic antennas to perform the test, whose measurement frequency-band range is from 9 kHz to 30 MHz. Fig. 14(a) shows the spectra of the received data from the two telescopic antennas, and the spectra of Channels 1 and 2 represent the radiated emissions of the DUT in the presence ambient noise. The radiated emissions of the equipment in this frequency band are obtained in the AC, as shown in Fig. 14(c). The comparison between Fig. 14(a) and (b) shows that from the qualitative point of view, the noise is greatly weakened after filtering and is well suppressed in a wide frequency band, which proves that the algorithm has a good noise-suppression effect in this frequency range. In addition, the comparison between Fig. 14(b) and (c) shows that the spectrum after the algorithm filtering is very close to that obtained from the AC test within a permissible error. We note that the Fig. 14(b) shows that the proposed algorithm has better performance than the conventional LMS algorithm. Compared with the results in the AC, we can observe that the proposed algorithm successfully cancels the ambient noise while preserving the DUT signal. The ambi-

TABLE III
FILTERING EFFECT OF THE TELESCOPIC ANTENNA IN THE TEST RANGE

Frequency /MHz	Amplitude before filtering /mV	Amplitude after filtering /mV	Amplitude in AC /mV	Filtering Effect /dB	Error /dB
0.009	42	40	48	−0.4238	−1.5836
0.4	50	1	1.1	−53.9794	−0.8279
0.75	12	0.8	0.9	−23.5218	−1.0231
1.4	10	1	1.2	−20	−1.5836
2.1	10	0.7	0.8	−23.0980	−1.1598

ent noise signals of 0.2 to 0.4 MHz are attenuated. In particular, the signal at 4 MHz is attenuated by 50 dB.

The comparison of the results at some frequency bins are listed in Table III. We select some typical frequency bins to analyze the effectiveness of the proposed algorithm from the quantitative point of view. In Table III, the signals at 9 kHz, 400 kHz, 750 kHz, 1.4 MHz, and 2.1 MHz are quantified. The algorithm shows the best filtering effect in the 400-kHz frequency. The background electromagnetic noise is suppressed by 54 dB, and the deviation from the test results in this frequency in the AC is less than 1 dB. In addition, the noises in the different frequencies are suppressed to varying degrees, proving that the algorithm can process complex noise in a wideband. The maximum measurement error between the proposed algorithm and the AC is 1.58 dB lesser than the 2 dB required in the frequency range from 9 kHz to 30 MHz, which demonstrates that the AC can be replaced by the proposed algorithm in this frequency range.

C. Test Results of Biconical Antenna

Similarly, we replace the two telescopic antennas with two biconical antennas in the measurement frequency-band range from 20 to 330 MHz to perform the equipment test in this frequency band. The three results are shown in Fig. 15(a)–(c). The first plot displays the spectra of the signals obtained from the near- and far-end antennas. The second plot displays the spectra of the output signals processed by the proposed and the conventional LMS algorithms. The last plot displays the spectra of the equipment signal in the AC.

Fig. 15(a)–(c) shows that a series of ambient noise exists whose amplitude is bigger than that of the equipment. Nevertheless, the proposed algorithm can cancel the ambient noise while the radiated emissions of the equipment are preserved. In contrast, the conventional LMS algorithm can cancel the ambient noise to an extent, but the amplitude of the ambient noise is larger than that of the equipment, which inevitably leads to serious errors in which the ambient noise is regarded as the signal of the equipment. The signals with a frequency of approximately 100 MHz are sharply weakened, and the electromagnetic spectrum after filtering is close to that obtained from the AC test, proving that the algorithm is effective in the frequency range of 20–330 MHz. Furthermore, we capture some typical frequency bins to analyze the results from the quantitative point of view. The quantitative analysis result is listed in Table IV. The

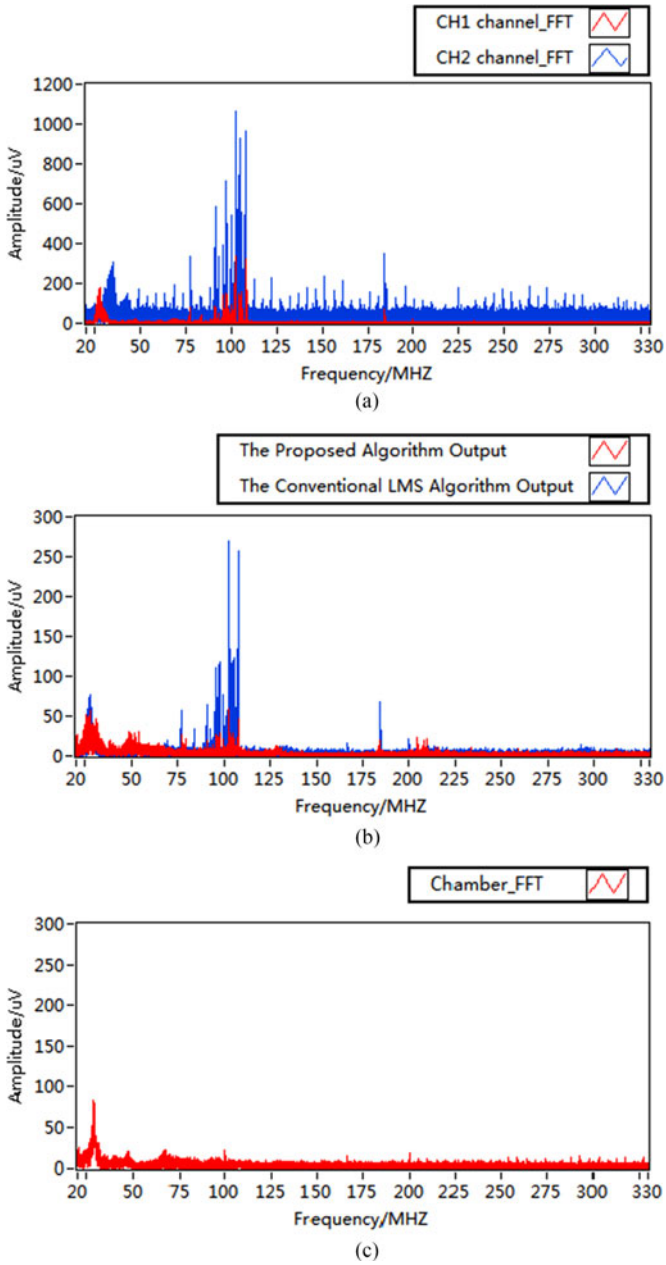

Fig. 15. Spectrum of the signal measured by a biconical antenna. (a) Spectrum of the signal (containing background noise). (b) Spectrum of the signal after filtering. (c) Spectrum of the signal in the AC.

TABLE IV
FILTERING EFFECT OF BICONICAL ANTENNA IN THE TEST RANGE

Frequency /MHz	Amplitude before filtering /μV	Amplitude after filtering /μV	Amplitude in AC /μV	Filtering effect /dB	Error /dB
25	300	100	120	−9.5424	−1.5836
75	90	10	12	−19.0849	−1.5836
100	180	40	30	−13.0643	2.4988
110	400	40	30	−20	2.4988
183	100	10	11	−20	−0.8279

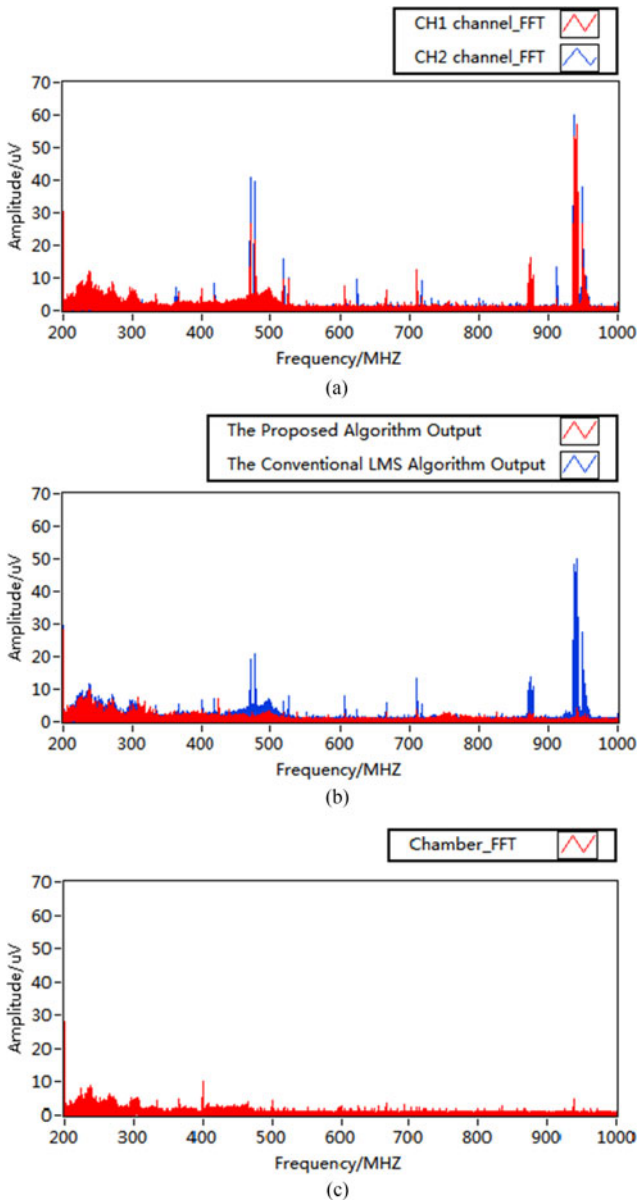

Fig. 16. Spectrum of the signal measured by a log-periodic antenna. (a) Electromagnetic spectrum (containing noise). (b) Spectrum of the signal after filtering. (c) Electromagnetic spectrum in the AC.

maximum measurement error between the proposed algorithm and in the AC is 2.5 dB lesser than the 6 dB required in the frequency range from 30 MHz to 1 GHz, which demonstrates that the AC can be replaced with the proposed algorithm in this frequency range.

D. Test Results of Log-Periodic Antenna

Finally, we use two log-periodic antennas instead of the above-mentioned two biconical antennas to perform the test whose measurement frequency-band range is from 200 MHz to 1 GHz. Fig. 16(a) shows the spectrum of the signal data received by the two antennas. The proposed algorithm is compared with the conventional algorithm shown in Fig. 16(b). The radiated emission of the equipment in the AC is shown in Fig. 16(c).

Fig. 16(a)–(c) shows that some spikes occur at 480, 520, 610, 660, and 870 MHz. The amplitudes of these signals are larger than those of the equipment. However, the proposed algorithm preserves the radiated emissions of the equipment, as shown in Fig. 16(c) (the spectrum of the signal in the AC is regarded as the radiated emissions of the equipment), and attenuates the ambient noise, which shows that the proposed algorithm can achieve good performance when subjected to strong interference. In contrast, the conventional LMS algorithm can suppress the ambient noise but not ideally. Furthermore, some typical frequency bins are selected to analyze the results from a quantitative point of view. The quantitative analysis result is listed in Table V. The maximum measurement error between the proposed algorithm and in the AC is 3.52 dB lesser than the 6 dB required in the frequency range from 30 MHz to 1 GHz, which shows that the AC can be replaced with the proposed algorithm in this frequency range.

E. Verification From the Point of View of the Electric Field Intensity

Since this paper focuses on the radiated emission of the large- and medium-sized electrical equipment, it is essential to discuss whether or not the results of the proposed algorithm accord with the requirements of the specification limits. In order to further verify the effectiveness of the proposed algorithm from another point of view of electric field intensity (dBμV/m), the impact on the antenna factor and cable loss is taken in account. Without loss of generality, we use electric field intensity received by the near end telescopic antenna with test frequency band range from 9 kHz to 60 MHz as an example. In fact, once the results of the proposed algorithm are consistent with those of AC within error permissibility, we can ensure electric field intensity computed by the spectrum results of the proposed algorithm below the specification limits. There are two main reasons:

1) The antennas and cable used to tests in AC and non-AC are identical with the same antenna factor and cable loss, respectively. Thus, the superposition of the antenna factor and cable loss has not influence on the relative error of electric field intensity from that of amplitude error according to (9).
2) Furthermore, the large- and medium-sized electrical equipment used for the experiment in the AC meet the requirements specification limits.

In summary, once the results of the proposed algorithm are consistent with those of AC within error permissibility, we can ensure electric field intensity computed by the spectrum results of the proposed algorithm below the specification limits on a basis of the above reasons. Especially, note that the figures use the semilogarithm coordinate system where dBμV/m is adopted as the basic unit of electric field intensity. To obtain electric field intensity of the equipment, the first step is that the vertical coordinate unit μ V of the amplitude spectrum is converted to dBμV. Second, antenna factor (dB(m^{-1})) is obtained by the curve fitting in LabVIEW. Finally, electric field intensity is computed by (9).

TABLE V
FILTERING EFFECT OF LOG-PERIODIC ANTENNA IN THE TEST RANGE

Frequency /MHz	Amplitude before filtering /μV	Amplitude after filtering /μV	Amplitude in AC /μV	Filtering effect /dB	Error /dB
480	25	2	3	−21.9382	−3.5218
520	10	1	1.2	−20	−1.5836
610	9	2	2.4	−13.0643	−1.5836
660	8	2	2.4	−12.0412	−1.5836
870	15	3	2.8	−13.9793	0.5993

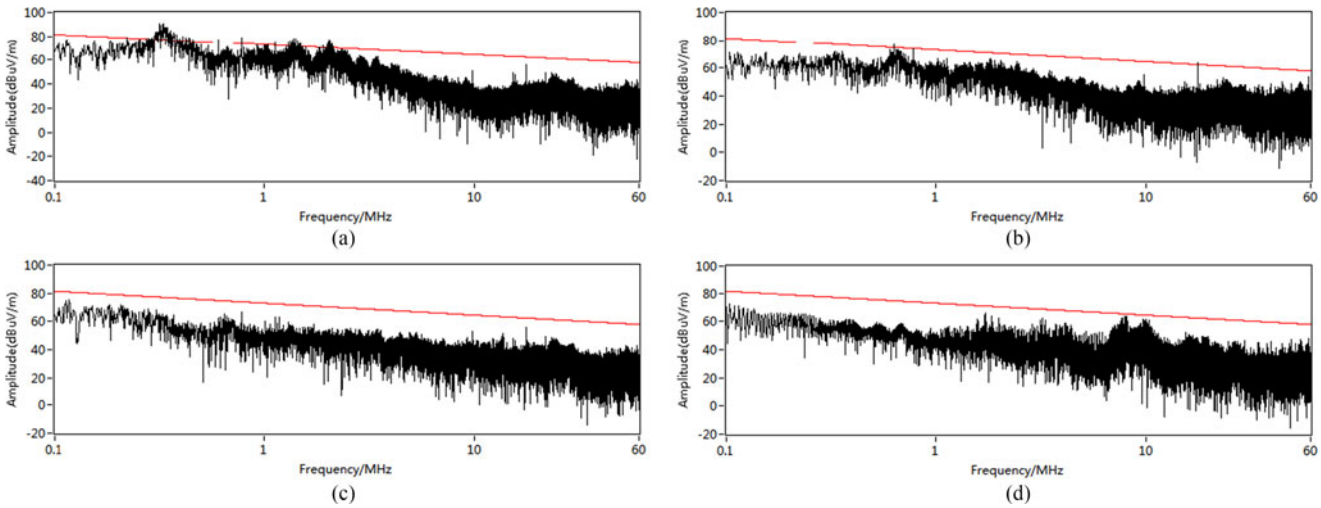

Fig. 17. Electric field intensity and the specification limits. (a) Electric field intensity of near end antenna. (b) Results of the conventional LMS algorithm. (c) Results of the proposed algorithm. (d) Results in AC.

As shown in Fig. 17, the first plot displays the electric field intensity of the signals obtained by the near end telescopic antenna, where the red line represents the specification limits. Obviously, electric field intensity of the radiated emissions consisting of the ambient noise does not meet the specification limits. By contrast, the conventional LMS algorithm suppress the ambient noise to large extent. Unfortunately, there are also a few electric field intensity of frequency bins above the specification limits, as shown in Fig. 17(b). Compared with the conventional LMS algorithm, electric field intensity filtered by the proposed algorithm accords with the specification limits in this context that the proposed algorithm are consistent with those of AC within error permissibility, as shown in Fig. 17(c). Moreover, the comparison of Fig. 17(c) and (d) illustrates the above reasons.

In conclusion, the above experimental result indicates that the electric field computed by the proposed algorithm are less than the electric field emissions limits over 9 kHz to 1 GHz frequency range. In view of this, the validity of the proposed algorithm is proved from the view of the electric field intensity. It can not only well modify the conventional LMS algorithm, but also perform the EMI measurements of the large- and medium-sized electrical equipment in the presence of ambient noise *in situ* instead of AC.

In summary, the algorithm can well eliminate the background noise in the frequency band of 9 kHz–1 GHz and can preserve the electromagnetic-radiation signal of the equipment. The filtering effect of the telescopic antenna in low frequencies can reach up to 53 dB, indicating that the electromagnetic noise of the equipment is most obvious in low band. The noise within the bands of the three antennas is weakened by different degrees, which not only proves the effectiveness of the algorithm but also shows that the electromagnetic noise has a wide frequency band. We note that the ambient noise in the frequency ranges from 9 kHz to 30 MHz, 20 to 330 MHz, and 200 MHz to 1 GHz correspond to the broadband, narrow band, and spikes, respectively.

We can prove that the proposed algorithm can be applied to suppress various noises such as broadband, narrowband, and spikes. The conventional LMS algorithm suffers from the difficulty in filtering out the noise in such a wide frequency band. We thus prove that the proposed algorithm performs well in the suppression of complex electromagnetic background noise. We can prove that the proposed algorithm can be applied to measure the radiated emissions of the large- and medium-sized electrical equipment instead of the AC.

V. CONCLUSION

In this paper, an intelligent adaptive filtering algorithm has been proposed and applied to test the electromagnetic radiated emissions of large- and medium-sized electrical equipment in the presence of ambient noises *in situ*.

This paper has presented our research on the elimination of the background electromagnetic noise of large- and medium-sized electrical equipment in the field tests. To overcome the defects of the traditional adaptive filtering method in

practical engineering applications, such as the wide frequency band of electromagnetic radiation and background electromagnetic noise, diverse frequencies, failure to ensure convergence rate and steady-state error, and difficult parameter adjustment, this work improves the traditional adaptive filtering algorithm and uses multiresolution analysis in the wavelet transform theory to decompose the tested band into wavelets. Then, it applies the improved adaptive filtering algorithm based on PSO to remove the noise in each decomposed band and eventually synthesizes all the processed bands to obtain the electromagnetic-radiation information of the equipment itself. This method has been verified by actual engineering application. It can well eliminate background noise and restore the electromagnetic-radiation signal of the equipment in the frequency band of 9 kHz–1 GHz, proving its effectiveness in filtering out the background noise of the equipment in complex electromagnetic environment.

This method can be applied in electromagnetic-radiation tests of equipment with system-level EMC, instead of using the AC. It has the following advantages:

1) The assembled equipment in the field does not need to be moved, and the electromagnetic-radiation test of the equipment can be performed under complex electromagnetic environment.
2) The test results are consistent with those in the AC with permissible error. Therefore, this method can help us to save the cost of constructing ACs, and it has a great market application value.
3) The proposed algorithm can significantly suppress various types of noises consisting of broadband, narrowband, and spikes.
4) The proposed algorithm can be applied in the frequency range from 9 kHz to 1 GHz. In particular, this algorithm can suppress the ambient noise below 30 MHz.

The algorithm provides excellent filtering effect on the offline data that do not have a high requirement in real time. However, the actual electromagnetic environment is time varying, and practical applications need electromagnetic-radiation information that is longer than just a few moment. Therefore, the algorithm still needs further improvement. Time–frequency analysis techniques such as the short-time Fourier transform can obtain the spectral information of the data and show the electromagnetic radiation of the equipment at different moments in the time axis. Thus, it can more comprehensively describe the electromagnetic radiation of the equipment than the FFT method.

For algorithm processing, this design eliminates the background noise in the near-end signals, and the obtained electromagnetic-radiation signal represents the electromagnetic radiation of the equipment in the near end. However, the electromagnetic radiation of the equipment is distributed in space, and the obtained electromagnetic-radiation description is not comprehensive. In the existing techniques [8], intelligent processing algorithm for multichannel blind signal can spatially filter out the background noise using signal processing methods such as the spatial spectrum estimation and adaptive broadband beamforming.

REFERENCES

[1] B. Zhang, Z. Yuan, and J. He, "Comparison on the test results between reverberation chamber and anechoic chamber," in *Proc. Asia-Pac. Symp. Electromagn. Compat.*, May 2012, pp. 769–772.

[2] A. Frech, S. Braun, and P. Russer, "Time-domain EMI measurements in the presence of ambient noise," in *Proc. IEEE Int. Symp. Electromagn. Compat.*, Aug. 2009, pp. 139–142.

[3] C. Osterwise, S. L. Grant, and D. Beetner, "Reduction of noise in near-field measurements," in *Proc. IEEE Int. Symp. Electromagn. Compat.*, Jul. 2010, pp. 171–176.

[4] A. Frech and P. Russer, "Real-time ambient noise cancellation for EMI measurements on open area test sites," in *Proc. Asia-Pac. Symp. Electromagn. Compat.*, May 2012, pp. 213–216.

[5] J. Xu, F. Dai, D. Su, Q. Qiao, and H. Zheng, "Ambient noise cancellation in frequency domain EMI measurement," in *Proc. 4th IEEE Int. Symp. Microw., Antenna, Propag. EMC Technol. Wireless Commun.*, Nov. 2011, pp. 555–558.

[6] S. Braun, T. Donauer, and P. Russer, "A real-time time-domain EMI measurement system for full-compliance measurements according to cispr 16–1-1," *IEEE Trans. Electromagn. Compat.*, vol. 50, no. 2, pp. 259–267, May 2008.

[7] Z. H. Lu, G. S. Li, D. M. Zhou, and P. G. Liu, "The time-frequency combination measurement method and its implementation for in-situ electronicmagnetic emission test," in *Proc. ISAPE*, Oct. 2012, pp. 861–864.

[8] Z. H. Lu, "A method for electromagnetic radiation emission test in electromagnetic interference environment," in *Proc. IEEE 6th Int. Symp. Microw., Antenna, Propag. EMC Technol.*, Oct. 2015, pp. 349–352.

[9] S. Braun, M. Al-Qedra, and P. Russer, "A novel realtime time-domain EMI measurement system based on field programmable gate arrays," in *Proc. 17th Int. Zurich Symp. Electromagn. Compat.*, Feb. 2006, pp. 501–504.

[10] W. W. Wu, Y. S. Wang, and J. C. Zhang, "An adaptive filter based on wavelet transform and affine projection algorithm," in *Proc. Int. Conf. Wavelet Anal. Pattern Recognit.*, Jul. 2010, pp. 392–397.

[11] Z. Dou, Q. Han, X. Niu, X. Peng, and H. Guo, "An adaptive filter for aeromagnetic compensation based on wavelet multiresolution analysis," *IEEE Geosci. Remote Sens. Lett.*, vol. 13, no. 8, pp. 1069–1073, Aug. 2016.

[12] S. Wu, Y. Shen, Z. Zhou, L. Lin, Y. Zeng, and X. Gao, "Research of fetal ECG extraction using wavelet analysis and adaptive filtering," *Comput. Biol. Med.*, vol. 43, no. 10, pp. 1622–1627, 2013.

[13] C. Feng, L. Zhang, and X. Hui, "A new adaptive filtering algorithm based on discrete wavelet transforms," in *Proc. 3rd Int. Congr. Image Signal Process.*, Oct. 2010, vol. 7, pp. 3284–3286.

[14] Z. WeiJun, "The research on LMS adaptive filter based on multi-scale domain," in *Proc. Int. Conf. Mechatronic Sci., Elect. Eng. Comput.*, Aug. 2011, pp. 2619–2622.

[15] X. See, K. Lee, W. Gan, and H. Li, "Proportionate subband adaptive filtering," in *Proc. Int. Conf. Audio, Lang. Image Process.*, Jul. 2008, pp. 128–132.

[16] A. Gilloire and M. Vetterli, "Adaptive filtering in subbands with critical sampling: Analysis, experiments, and application to acoustic echo cancellation," *IEEE Trans. Signal Process.*, vol. 40, no. 8, pp. 1862–1875, Aug. 1992.

[17] Y. Chen, J. Tian, and Y. Liu, "Variable step size LMS algorithm based on modified sigmoid function," in *Proc. Int. Conf. Audio, Lang. Image Process.*, Jul. 2014, pp. 627–630.

[18] S. Roy and J. J. Shynk, "Analysis of the momentum LMS algorithm," *IEEE Trans. Acoust., Speech, Signal Process*, vol. 38, no. 12, pp. 2088–2098, Dec. 1990.

[19] D. T. M. Slock, "On the convergence behavior of the LMS and the normalized LMS algorithms," *IEEE Trans. Signal Process.*, vol. 41, no. 9, pp. 2811–2825, Sep. 1993.

[20] S. Attallah, "The wavelet transform-domain LMS adaptive filter with partial subband-coefficient updating," *IEEE Trans. Circuits Syst. II, Express Briefs*, vol. 53, no. 1, pp. 8–12, Jan. 2006.

[21] S. S. Pradham and V. U. Reddy, "A new approach to subband adaptive filtering," *IEEE Trans. Signal Process.*, vol. 47, no. 3, pp. 655–664, Mar. 1999.

[22] C. Zhiyuan and Y. Guangxin, "LMS algorithm based on subband decomposition," in *Proc. Int. Conf. Commun. Technol. Proc.*, Oct. 1998, vol. 1, pp. 128–133.

[23] S. G. Mallat, "A theory for multiresolution signal decomposition: The wavelet representation," *IEEE Trans. Pattern Anal. Mach. Intell.*, vol. 11, no. 7, pp. 674–693, Jul. 1989.

[24] D. J. Krusienski and W. K. Jenkins, "A modified particle swarm optimization algorithm for adaptive filtering," in *Proc. IEEE Int. Symp. Circuits Syst.*, May 2006, pp. 4 pp.–140.
[25] D. J. Krusienski and W. K. Jenkins, "Particle swarm optimization for adaptive IIR filter structures," in *Proc. Congr. Evol. Comput.*, 2004, vol. 1, pp. 965–970.
[26] J. Robinson and Y. Rahmat-Samii, "Particle swarm optimization in electromagnetics," *IEEE Trans. Antennas Propag.*, vol. 52, no. 2, pp. 397–407, Feb. 2004.
[27] S. U. Khan, S. Yang, L. Wang, and L. Liu, "A modified particle swarm optimization algorithm for global optimizations of inverse problems," *IEEE Trans. Magn.*, vol. 52, no. 3, pp. 1–4, Mar. 2016.
[28] A. T. Al-Awami, A. Zerguine, L. Cheded, A. Zidouri, and W. Saif, "A new modified particle swarm optimization algorithm for adaptive equalization," *Digit. Signal Process.*, vol. 21, no. 2, pp. 195–207, 2011.

Liu Sheng was born in 1957. He received the B.Eng. degree in industrial automation from Harbin University of Civil Engineering and Architecture, Harbin, China, on February 1982, and the Master's and Doctoral degrees both in theory and control engineering from Harbin Engineering University, Harbin, on March 1982 and 2000, respectively.

He is currently a Professor at Harbin Engineering University. His current research interests include electromagnetic compatibility prediction and measurement, optimization estimate and control of random system, robust control and ship control system, etc.

Wang Bangmin received the B.Sc. degree in theory and control engineering from Harbin Engineering University, Harbin, China, in 2014. He is currently working toward the Doctoral degree in electromagnetic compatibility prediction and measurement and electromagnetic compatibility signal processing, from Harbin Engineering University.

Zhang Lanyong received the Doctoral degree at Harbin Engineering University, Harbin, China, in 2011.

He has been a Postdoctoral Researcher of electromagnetic compatibility at Harbin Engineering University, Harbin, China. He is currently a Master's Supervisor at Harbin Engineering University, and majors in electromagnetic compatibility prediction and measurement and stochastic signal processing. His current research interests include the fast transient analysis and modeling of field-excited multiconductor networks, power-line carrier propagation, electromagnetic field interference from overhead multiconductor lines, and electromagnetic interaction with advanced composite materials. He received the Excellent Graduate Award from Harbin Engineering University, on August 2009.